Reducing Non-rigidity in TLS Point Clouds Induced by Inhomogeneous Systematic Errors Using Free-form Surface Modeling

Yihui Yang[1], Corinna Harmening[2], Daniel Czerwonka-Schröder[3], Christoph Holst[1]

[1] Chair of Engineering Geodesy, TUM School of Engineering and Design, Technical University of Munich, Arcisstraße 21, 80333 Munich, Germany – (yihui.yang, christoph.holst)@tum.de
[2] Geodetic Institute, Karlsruhe Institute of Technology, Englerstraße 7, 76131 Karlsruhe, Germany – corinna.harmening@kit.edu
[3] Department of Geodesy, Bochum University of Applied Sciences, Am Hochschulcampus 1, 44801 Bochum, Germany – Daniel.Czerwonka-Schroeder@hs-bochum.de

Keywords: Terrestrial Laser Scanning, Monitoring, Refraction, B-spline Surface, Planar Patches, M3C2 Distance.

Abstract

In geodetic monitoring, terrestrial laser scanning (TLS) point clouds are typically assumed to be accurate and true-to-scale, implying that data acquired from different epochs or stations differ only by rigid transformations. Consequently, systematic errors related to scanner or platform variations can be mitigated through rigid point cloud registration. However, variations in the propagation speed and path of laser beams due to atmospheric refraction, as well as ranging biases induced by surface properties, can introduce non-rigid distortions in the generated point clouds. These effects are particularly pronounced under complex meteorological and topographic conditions, such as in mountainous areas. As a result, the acquired point clouds exhibit inhomogeneous and non-linear deviations that cannot be effectively compensated by simple distance corrections or rigid transformations. In this study, robust rigid registration is first performed to minimize the effects of platform offsets. A data-driven approach is then employed to generate sparse stable points, providing distance deviations that incorporate spatially varying systematic errors. Finally, a free-form surface is fitted to these sparse point-wise distance deviations, thereby establishing a 3D correction field for the entire point cloud. For a dataset collected by a permanent TLS monitoring system in the Vals Valley (Tyrol, Austria), the proposed method effectively reduces the registration residuals in TLS point clouds caused by inhomogeneous systematic errors.

1. Introduction

Geodetic monitoring based on terrestrial laser scanning (TLS) technology has made significant progress over the past two decades. Particularly, permanent laser scanning (PLS), as the station-fixed and continuous operation of TLS, has emerged as a powerful tool for monitoring active natural disasters in recent years. PLS achieves higher spatial and temporal resolution compared to traditional monitoring methods, such as GNSS and total station (Czerwonka-Schröder, 2023; Lindenbergh et al., 2025). Accordingly, developed change detection and analysis algorithms support the revelation of complex surface dynamics and the early warning of potential risks (Anders et al., 2020; Kuschnerus et al., 2024; Yang and Holst, 2025a).

Despite the advantages of PLS in monitoring tasks, unexpected errors (including systematic and random) may occur in the generated scans during long-term measurements. Typically, random errors can be reduced by averaging multiple measurements or local patches, whereas identifying and mitigating systematic errors remain a challenge (Yang et al., 2025). These systematic errors mainly come from the following sources (Soudarissanane et al., 2011; Kuschnerus et al., 2021):

- Uncalibrated instrument
- Unstable platform
- Atmospheric refraction
- Scanned surface properties
- Scanning geometry
- Georeferencing/Registration

The systematic errors may be misinterpreted as surface deformations if they are not considered, detected, and eliminated, leading to incorrect decision-making. Thereby, these errors appearing in laser scanning point clouds should be mitigated before conducting change detection or deformation analysis.

Assuming that the laser scanner is well calibrated, and based on the analysis of continuous total station measurements, Yang et al. (2025) approximated the comprehensive impact of systematic errors as rigid-body movements of the entire scan, thus mitigating these systematic deviations using rigid point cloud registration. Under the assumption that atmospheric refraction consistently affects laser measurements over the scanned area, this method was successfully applied to mitigate systematic errors of the point clouds acquired by a PLS system from several centimeters to the millimeter level in a rockfall monitoring case (Yang et al., 2025). However, due to the complex topography and significant diurnal temperature variations in mountainous regions, atmospheric conditions across the monitored area may exhibit pronounced spatial and temporal inconsistencies. The resulting spatially inhomogeneous systematic errors cannot be eliminated through rigid registration.

Specifically, the atmospheric refraction influences the speed and path of laser propagation in a systematic way, and it is related to the change of meteorological parameters (e.g., temperature, air pressure, and humidity), as well as to the measuring distance and the geometry of monitored surfaces (Friedli, 2020; Yang et al., 2025). Systematic errors in point cloud data caused by atmospheric refraction are particularly noticeable (from a few millimeters to several centimeters) in mountainous terrain at long ranges (Friedli et al., 2019; Voordendag et al., 2023).

Several recent studies have focused on the mitigation of atmospheric refraction-induced measurement errors by employ-

This contribution has been peer-reviewed. The double-blind peer-review was conducted on the basis of the full paper.
https://doi.org/10.5194/isprs-annals-XI-1-2026-419-2026

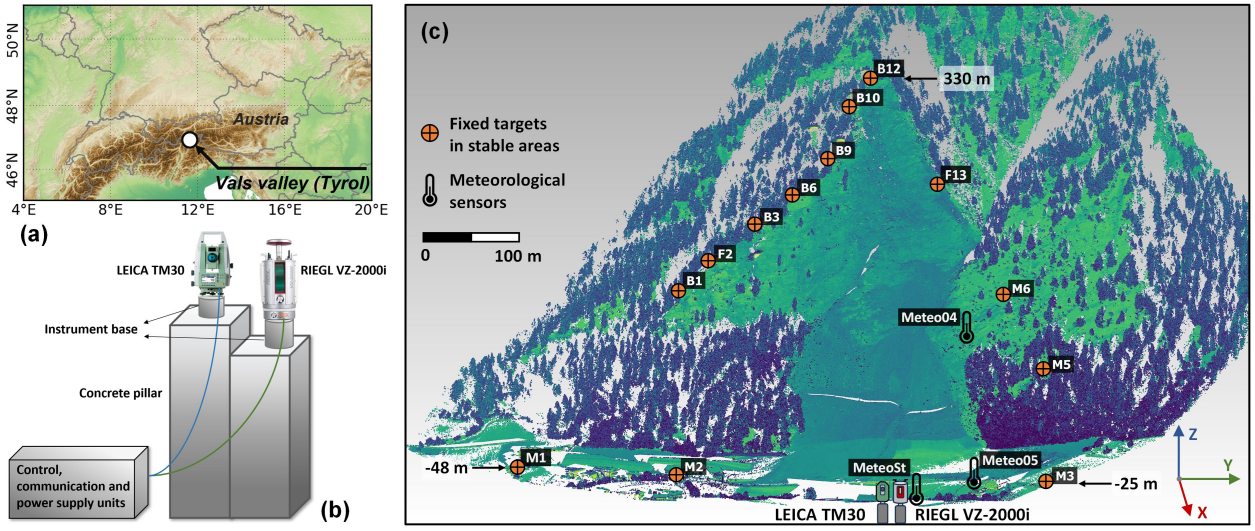

Figure 1. Overview of the rockfall and the monitoring system in the Vals Valley: (a) Location of the rockfall; (b) Setup of the monitoring system; (c) Captured point cloud and the distribution of targets and sensors.

ing meteorological models or numerical simulation approaches. One branch of these strategies constructs 3D refractive-index models by integrating meteorological sensor networks with spatial interpolation or ray-tracing simulations. For example, based on a network of meteorological sensors deployed in the monitored areas, García-Asnejo et al. (2025) built a 3D refractivity model and subsequently applied it to long-range TLS data. Similar studies can also be found in Luján et al. (2025), which employed multi-source meteorological data and a digital terrain model for more precise calculations of distance and vertical angle corrections. Other studies use established refractivity functions combined with numerical integration of the ray path through vertically stratified atmosphere (Friedli, 2020; Voordendag et al., 2023).

In these meteorological/physical-model approaches, the major advantages are the physical interpretability of the correction (i.e., tying errors to known atmospheric parameters) and the ability to apply the model to all points in the scan. However, drawbacks include the need for sufficiently dense meteorological measurement or high-resolution atmospheric model data, the computational cost of ray-tracing integrations, and potentially insufficient modeling of small-scale variability (e.g., turbulence, local micro-climate), which may still produce residual non-rigidities in the point cloud.

To address these limitations, we propose a straightforward approach to reduce the influence of inhomogeneous systematic errors in TLS point clouds. Specifically, we

- utilize automatically extracted stable points containing systematic errors and
- generate a 3D continuous correction field by free-form surface modeling,
- thereby reducing the remaining non-rigid deviations in the point cloud after rigid registration.

This alternative offers a purely data-driven correction strategy when full meteorological sensor networks or high-resolution atmospheric models are unavailable.

The remainder of this paper is organized as follows: Section 2 describes the monitoring system and the used dataset. Section 3 presents the proposed method for correcting systematic errors. Section 4 demonstrates the evaluation results on four selected scans. Section 5 discusses the limitations and potentials of the method, followed by conclusions in Section 6.

2. Monitoring System and Data Description

As illustrated in Figure 1, a PLS system equipped with a RIEGL VZ-2000i laser scanner was deployed in the Vals Valley (Tyrol, Austria) to continuously monitor a rockfall surface (Schröder et al., 2022). Several artificial targets (prisms) were fixed in the stable areas surrounding the rockfall surface and in the valley area. A total station (LEICA TM30) was also installed next to the laser scanner to measure the prisms simultaneously (see Figure 1(b)). The measurement distance is up to 800 m. Both instruments were installed on a concrete pillar.

In addition, three meteorological sensors were set up to derive correction information for range measurements of two instruments, including one beside the scanner (MeteoSt), one in the middle of the rockfall surface (Meteo04), and one in the valley area (Meteo05). We select the data from four days in May 2021, during which atmospheric refraction effects were stronger, to analyze the behaviors of systematic errors in captured point clouds. Figure 2 shows the derived ppm (parts per million) values from the meteorological sensors. These values reflect the impact of atmospheric conditions on distance measurements and generally exhibit consistent diurnal variations. However, due to differences in location, parameters such as temperature show systematic or random variations, leading to spatially inconsistent ranging differences. Figure 2 also displays the differences after distance correction using ppm values from Meteo04 and MeteoSt, with the maximum difference reaching up to 7 mm.

Therefore, using limited meteorological observations to correct distance measurements may become ineffective when atmospheric conditions exhibit strong spatial variability. This spatial inconsistency becomes increasingly pronounced with longer measurement ranges, while the deployment of dense meteorological sensor networks is often impractical due to cost and maintenance constraints.

This contribution has been peer-reviewed. The double-blind peer-review was conducted on the basis of the full paper.
https://doi.org/10.5194/isprs-annals-XI-1-2026-419-2026 | © Author(s) 2026. CC BY 4.0 License.

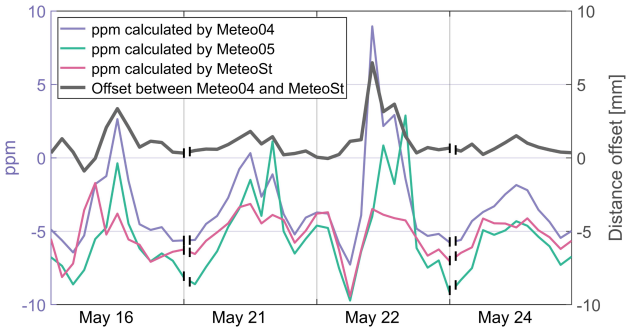

Figure 2. Difference in derived ppm value from different meteorological sensors and caused distance offsets.

The total station measurements of the distributed prisms were also analyzed, and a high degree of consistency among the measured values was reported in Yang et al. (2025). We further attempted to correct the polar coordinates of scan points using synchronized total station observations. However, the prism distribution in this dataset is too sparse, particularly in the central portion of the rockfall surface where no targets were installed, resulting in these areas being under- or over-corrected by the derived correction fields. Moreover, the systematic errors caused by atmospheric refraction captured by the total station may differ in magnitude from corresponding point cloud deviations, thus requiring additional scaling and realignment steps.

3. Methods

To further reduce the residual systematic errors – particularly those induced by atmospheric refraction – after precise registration, we propose a data-driven distance correction strategy that relies solely on the point cloud data itself. This approach is established under the following assumptions:

(1) The laser scanner is well calibrated, and the remaining instrument-related errors are negligible.
(2) Most of the overlapping regions between the point clouds remain stable; that is, the small surface distances observed in these regions originate from measurement errors rather than actual deformations.
(3) Systematic errors arising from atmospheric refraction have a greater impact on distance measurements than on angular measurements.

The overall workflow is illustrated in Figure 3. The captured point cloud is first registered to a reference scan (i.e., the initial epoch) in a robust way (Section 3.1). Stable areas between the two aligned point clouds are then identified by generating and selecting planar patches. The normal distances between the nearest corresponding patches are projected onto the line of sight to obtain the distance deviations (Section 3.2). After filtering, a B-spline surface is fitted to these deviations in 3D space to establish a spatial distance correction field, which is subsequently applied to adjust each point in the registered scan (Sections 3.3 and 3.4). The details of each step are described in the following subsections.

3.1 Robust Rigid Registration

Accurate and robust registration is essential, as this step can minimize the rigid-body motions of the point cloud caused by changes in the monitoring platform, as well as reduce the linear

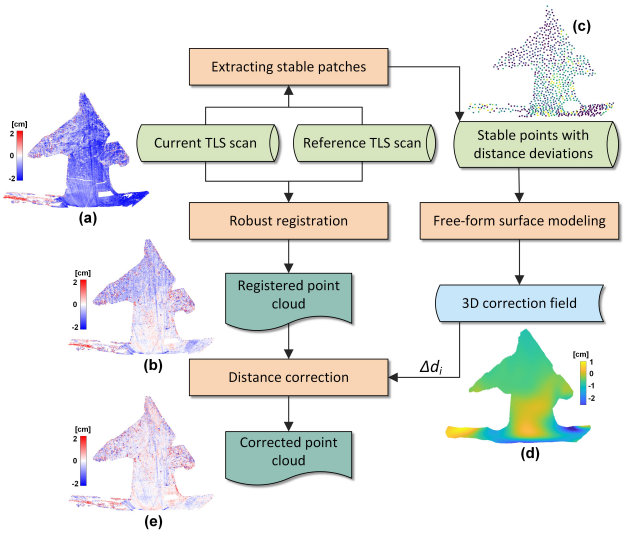

Figure 3. Workflow of the proposed correction method for TLS point clouds. (**a**) shows the surface deviations of the raw scan due to various systematic errors, (**b**) shows the surface deviations after rigid registration, (**c**) presents the extracted stable points, (**d**) displays the distance correction field by B-spline surface modeling, and (**e**) shows the final registered and corrected scan.

component of the ranging bias induced by atmospheric refraction (Yang et al., 2025). The Piecewise-ICP algorithm is employed to align the raw data with the reference scan, reporting millimeter-level registration accuracy for this dataset (Yang and Holst, 2025b). This targetless registration framework automatically identifies stable planar areas and performs an enhanced point-to-plane ICP, making it robust against outliers and potential local deformations. Figure 4 presents an example of identified stable planar areas on the rockfall surface, which are used for rigid registration in the Piecewise-ICP algorithm. Further methodological details can be found in Yang and Holst (2025b).

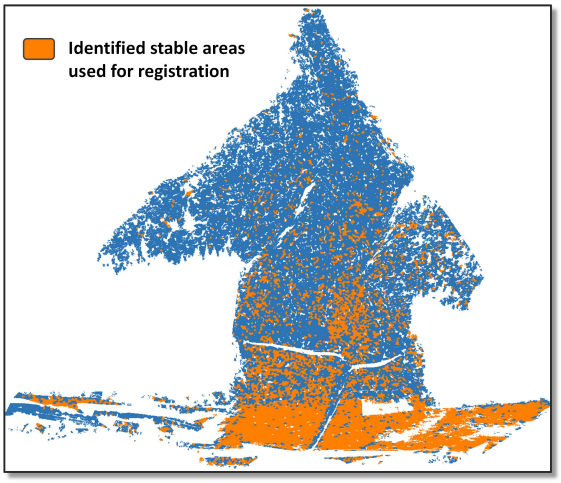

Figure 4. Identified stable and planar areas by Piecewise-ICP for transformation estimation.

To ensure that the registration process is not affected by noise, outliers, and potential deformations, Piecewise-ICP utilizes only a subset of the stable areas that are highly reliable to estimate the rigid transformation. Consequently, many points that could otherwise be considered stable are excluded from the re-

gistration process. For example, only a few regions in the upper part of the surface are used for registration in Figure 4, as these areas exhibit high surface roughness and vegetation-induced outliers, despite no deformations having occurred there. To improve the spatial coverage and resolution of the derived correction field, the stable points must be reproduced from the registered scans, and then distance deviations can be computed at these locations.

3.2 Extraction of Stable Points with Distance Deviations

As discussed in Section 3.1, stable points with higher spatial resolution need to be re-generated from the registered scans. Assuming that the stable points are primarily located in planar and overlapping regions between the reference and current epochs, a supervoxel-based segmentation followed by a refined selection procedure is exploited to extract stable patches (Yang, 2023). This selection process removes patches with insufficient point density, low planarity, or high linearity. Subsequently, the normal distances between the centroids of the nearest corresponding patches are calculated. Patches with normal distances exceeding a predefined threshold (empirically set to 2 cm in this study) are discarded, as they are considered unstable.

As illustrated in Figure 5, let $\mathbf{n}_{\text{invLoS}}$ denote the vector in the opposite direction to the line of sight (i.e., $\mathbf{n}_{\text{invLoS}} = (-x_i, -y_i, -z_i)$), $\mathbf{n}_{\text{NorSt}}$ the normal vector of a stable patch in the reference scan (reoriented toward the scanner), and d_{Nor} the signed normal distance between the nearest patches (positive d_{Nor} indicates facing the scanner, while negative d_{Nor} indicate facing the line of sight). The projected distance along the line of sight is then computed as

$$\Delta d = \frac{d_{\text{Nor}}}{\cos\theta} = \frac{d_{\text{Nor}} \cdot |\mathbf{n}_{\text{NorSt}}| \cdot |\mathbf{n}_{\text{invLoS}}|}{\mathbf{n}_{\text{NorSt}} \cdot \mathbf{n}_{\text{invLoS}}}, \tag{1}$$

where Δd represents the distance deviation for the centroid of the patch in the current scan (positive values indicate toward the scanner), and θ is the angle between $\mathbf{n}_{\text{NorSt}}$ and $\mathbf{n}_{\text{invLoS}}$.

To further mitigate the influence of potential noise (e.g., from distance or normal vector calculations) on subsequent processing, we apply a voxel-based downsampling to generate uniformly distributed stable (voxel) points. For each voxel, only the stable point with the median distance deviation is retained as input for constructing the correction field, thus filtering out more noisy points. The negative of these distance deviations ($-\Delta d$) at the corresponding points is then used as the correction values for the current epoch scan.

3.3 Free-form Surface Modeling

Free-form surfaces like B-splines have become a standard tool in the context of point cloud modeling (Bureick et al., 2016; Kermarrec et al., 2020). Due to their flexibility, they are able to represent even complex objects, whereas their locality makes them particularly suitable for deformation modeling (Ötsch et al., 2023; Aichinger and Schwieger, 2022).

A B-spline surface is defined by Piegl and Tiller (1995):

$$\mathbf{S}(u,v) = \sum_{i=0}^{n_P} \sum_{j=0}^{m_P} N_{i,p}(u) \cdot N_{j,q}(v) \cdot \mathbf{P}_{i,j}, \qquad u,v = [0,\ldots,1]. \tag{2}$$

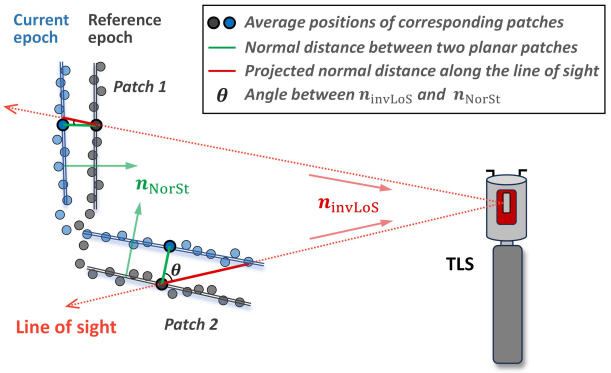

Figure 5. Calculation of the distance correction values for extracted stable patches.

According to Equation 2, a surface point $\mathbf{S}(u,v)$ is computed as the weighted average of a bidirectional net of control points $\mathbf{P}_{i,j}$. The respective weights are defined by B-spline basis functions $N_{i,p}(u)$ and $N_{j,q}(v)$ with degrees p and q, respectively. These basis functions can be computed recursively (Piegl and Tiller, 1995).

When using B-spline surfaces to model point clouds, typically only the position of the control points is estimated in a linear Gauss-Markov model (Bureick et al., 2016). The optimal number of control points $(n_P + 1) \cdot (m_P + 1)$ can be determined by information criteria (Harmening and Neuner, 2016, 2017). The use of structural risk minimization enables to also include the degrees of the basis functions into the model selection task (Harmening, 2020). Otherwise, the choice of cubic B-splines is generally accepted (Piegl and Tiller, 1995). Additionally, surface parameters u and v have to be allocated to the observations, which can be done by means of a base surface parameterization (Harmening and Neuner, 2015).

3.4 Point Cloud Correction

The input for building a 3D distance correction field is a sparse 4D point cloud that contains the Euclidean coordinates $[x_i, y_i, z_i]$ of each stable voxel point as well as the corresponding correction value $-\Delta d_i$, $i = 1, ..., n_V$, with n_V being the number of voxels, as stated in Section 3.2. Since these are initial investigations, this 4D point cloud is converted into a 3D point cloud $[x_i, y_i, -\Delta d_i]$, assuming that x and y-coordinates are sufficient for capturing the spatial distribution of the correction values. The limitations of this simplified approach and its further development will be discussed in Section 5.2.

This 3D point cloud is then modeled by means of a B-spline surface as described in Section 3.3. The resulting surface provides spatially continuous information about corrections to be applied to the distance measurements of the registered scan. In order to allocate a correction value to each data point of the original point cloud, their x_j and y_j coordinates are used to find the corresponding correction value $-\Delta d_j$ via the correction surface ($j = 1, ..., n$, n = number of data points). This correction value is then used to correct the corresponding distance measurement in the polar coordinate system.

4. Experimental Results

The proposed workflow is evaluated using four selected epochs from the dataset described in Section 2. According to the

total station measurements, these epochs exhibit potentially strong and spatially inhomogeneous refraction effects. Non-rigid distortions can be observed when comparing these scans with the reference scan after accurate registration has been performed. The reference epoch corresponds to 01:00 on 2021-05-16, while the selected epochs are 01:00 and 13:00 on 2021-05-22 and 2021-05-24, representing nighttime and daytime conditions with the lowest and highest temperatures, respectively. Prior to processing, most vegetation areas surrounding the rockfall surface and significantly changed regions were manually cropped out.

4.1 Evaluation Metrics

In this study, the performance of the proposed pipeline is evaluated based on the surface distances between the corrected point cloud and the reference scan within stable areas, where smaller distances indicate higher correction accuracy. The M3C2 (Multiscale Model-to-Model Cloud Comparison) distance metric is adopted due to its robustness to noise and non-uniform point spacing (Lague et al., 2013).

Since the registration algorithm achieves millimeter-level accuracy, the remaining systematic errors caused by factors such as refraction and surface properties are small but exhibit local spatial consistency. Therefore, the point cloud surface is divided into several regions for separate evaluation. Frequency distribution histograms of the M3C2 distances for all points in each region are generated, and the statistical characteristics are compared among three cases: (1) without registration and correction, (2) with registration only, and (3) with registration combined with distance correction.

4.2 3D Distance Correction Fields

Based on the extracted and filtered stable points with corresponding distance correction values, B-spline surface modeling is applied to generate a continuous 3D correction field for each scan. The voxel size is set to 6 m for downsampling and filtering, resulting in approximately 4,000 points being used for surface modeling. To enhance the local fitting performance while suppressing noise effects, a B-spline surface with 6×6 control points is employed. The derived distance correction fields for the four selected scans are presented in Figure 6. It should be noted that these correction values are influenced not only by atmospheric refraction but also by residual registration errors, surface properties, and the scanning geometry (e.g., varying incidence angles). Analyzing the error budget from these factors is beyond the scope of this paper.

The correction fields of the four epochs exhibit generally consistent spatial patterns. Most upper-slope areas show deviations of approximately 5 mm toward the line of sight, which can be attributed to increased distance measurements under lower air temperatures at higher altitudes. In contrast, the middle regions display only minor deviations, with correction values close to zero. The conditions within the valley are more complex and spatially heterogeneous: the left side of the valley shows positive deviations (toward the scanner), whereas the right side exhibits substantially lower negative values. This spatial inconsistency is likely related to uneven temperature distribution on the ground in the valley area. However, a detailed physical explanation for these significant differences remains unavailable and warrants further investigation.

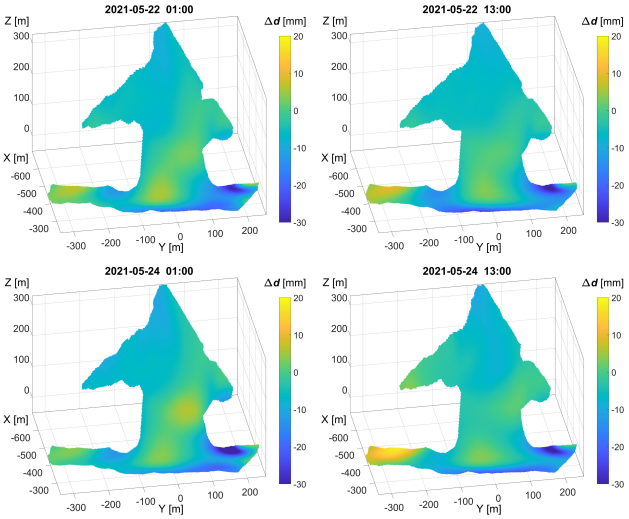

Figure 6. 3D distance correction fields of four epochs derived by B-spline surface modeling (displaying only the data area).

4.3 Comparison of M3C2 Distances

As described in Section 4.1, the performance of the proposed method is evaluated by computing and statistically analyzing the M3C2 distance distributions in local regions before and after correction. For comparison, the distance distribution prior to registration is also presented in a frequency histogram.

As shown in Figure 7, the M3C2 distances between the reference scan and precisely registered scans are illustrated over the entire point cloud surfaces (see the left column). Distinct systematic deviations are observed, particularly in the upper areas and the lower-right corner across all epochs, although their magnitudes are only several millimeters. The negative M3C2 distances in these areas indicate that the surface shifts toward the line of sight, which is likely due to increased distance measurements.

To quantify the systematic errors within specific areas, the point cloud surface is divided into four regions based on elevation. According to the scanner’s local coordinate system, Area 1 corresponds to the region above 100 m, Area 2 represents the middle section from 0 m to 100 m, while Areas 3 and 4 denote the left and right sides of the valley below 0 m, respectively.

The right column in Figure 7 presents the M3C2 distance histograms, providing a quantitative assessment of the surface deviations in four different parts. Before registration, the M3C2 distances exhibit broad distributions with significant offsets, indicating misalignment between epochs. After applying the Piecewise-ICP registration, the distributions become significantly narrower, and the mean values decrease noticeably. However, noticeable systematic errors remain, especially in the upper region (Area 1) and the right side of the valley (Area 4), which cannot be fully compensated by rigid registration.

After applying the proposed distance correction method, the histograms in Areas 1, 2, and 4 exhibit clear improvements. The distributions become more centralized, and the mean M3C2 distances approach zero, indicating that the systematic errors are effectively reduced. As the residual systematic errors in this dataset are relatively small, we use percentages to assess the correction performance. The mean distance after correction decreases by approximately 23–28% in Area 1 and 27–36% in

https://doi.org/10.5194/isprs-annals-XI-1-2026-419-2026

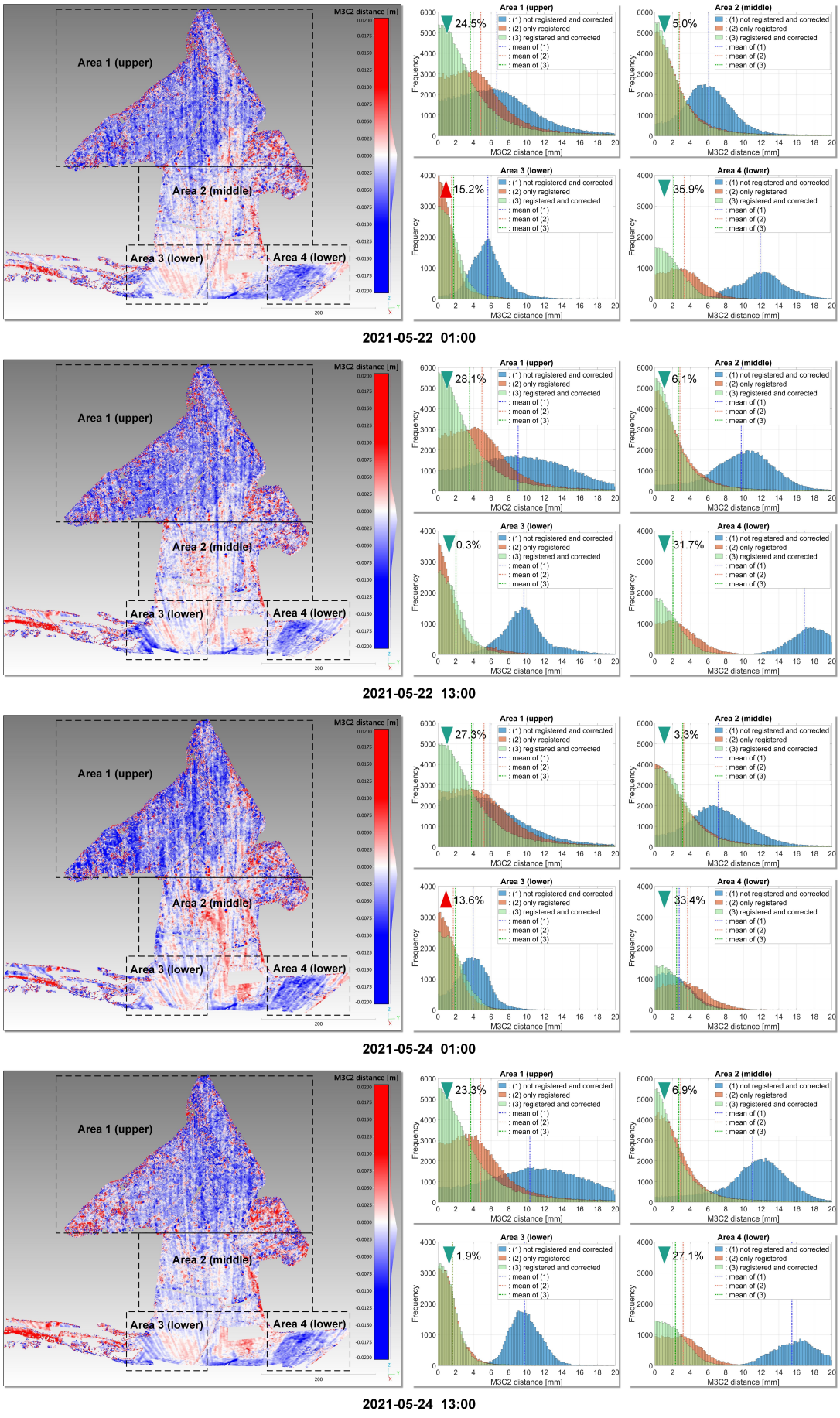

Figure 7. Comparison of M3C2 distance between four selected scans (before registration, after registration, and after registration + distance correction) and the reference scan on 2021-05-16. The left column shows the 3D distribution of M3C2 distance residuals after registration only, while the right column displays the histogram of M3C2 distances after robust registration and/or distance correction.

This contribution has been peer-reviewed. The double-blind peer-review was conducted on the basis of the full paper.
https://doi.org/10.5194/isprs-annals-XI-1-2026-419-2026 | © Author(s) 2026. CC BY 4.0 License.

Area 4, compared to the uncorrected case. In contrast, Areas 2 and 3, which originally exhibit smaller deviations, show relatively minor changes after correction, confirming that the proposed method does not introduce artificial distortions in already stable regions. It is worth noting that in Area 3 of the first and third epochs, the mean M3C2 distances slightly increase after correction. This counter-effect is likely due to the minimal original systematic bias in this area. The mean change after correction is less than 0.5 mm, indicating that the effect is negligible and does not adversely affect the overall correction performance.

Overall, M3C2-based statistical evaluation verifies that the proposed correction pipeline can effectively mitigate the remaining inhomogeneous systematic errors after rigid registration – particularly those induced by strong atmospheric refraction – while preserving the geometric consistency of undistorted areas.

5. Discussion

In this section, we discuss the modeling quality of the B-Spline surface (Section 5.1) as well as limitations and potentials of our approach (Section 5.2).

5.1 Modeling Quality of the B-spline Surface

The quality of the results is to a large extent determined by the ability of the B-spline surface to represent the correction field. In this study, two difficulties have arisen in this context. The generated point clouds $[x_i, y_i, -\Delta d_i]$ that form the basis for the B-spline estimation are considerably noisier than typical TLS point clouds. Therefore, a visual evaluation of the chosen complexity of the B-spline model is difficult. Model selection criteria can also be used to choose the optimal complexity in this context (Harmening and Neuner, 2017). However, due to the convex boundaries of the investigated point cloud, the base surface parameterization using Coons Patch reaches its limit (Harmening and Neuner, 2015).

Especially when choosing more complex B-spline surfaces, artifacts emerge in the boundary regions that considerably influence the correction values. For this reason, comparatively simple B-spline surfaces with 6×6 control points have been chosen in order to investigate the general applicability of the approach. Alternative parameterization strategies (e.g., local parameterization as proposed by Harmening and Butzer (2024)) might improve the approximation quality of the B-spline models and might also provide the basis for the estimation of more complex B-spline models. These relationships will be investigated in future work.

5.2 Limitations and Potentials

Although the proposed point cloud–based correction strategy effectively reduces the non-rigid distortions caused by inhomogeneous systematic errors in the Vals Valley dataset, several limitations should be acknowledged.

First, the method assumes that the major part of the scanned surface is stable relative to the reference epoch. Under this assumption, the extracted stable regions are expected to represent (both random and systematic) measurement errors rather than real deformations. Therefore, the approach is unsuitable for scenarios involving large-scale movements or deformations. Second, the proposed correction strategy is merely distance-based and thus cannot address systematic angular errors. In cases of severe atmospheric refraction causing significant non-uniform laser beam deflection, the method is unable to detect or correct the corresponding angular biases. Deploying denser target networks and integrating precise total station observations may help to quantify and compensate for such angular deviations. Finally, the current B-spline correction field assumes that the horizontal coordinates can directly represent any position within the scan, which may be inadequate for surfaces with vertical structures. Future work will focus on developing a spatial correction field based on 3D coordinate mapping.

Although the degree of non-rigidity observed in the present dataset is relatively minor, the proposed method offers a practical and scalable solution for long-range monitoring scenarios (e.g., beyond 1 km), where atmospheric refraction can induce stronger spatial distortions in TLS point clouds. In addition, with the increasing availability of temporally dense correction fields, machine learning techniques could be employed to identify underlying patterns in refraction-induced deviations. Such data-driven analysis would enable the prediction of time-dependent correction models, ultimately paving the way toward automated atmospheric refraction compensation without the need for physical targets or external sensors.

6. Conclusions

This study proposes a data-driven correction strategy to reduce non-rigid distortions in TLS point clouds caused by spatially varying systematic errors in the context of geodetic monitoring. The approach integrates robust Piecewise-ICP registration with free-form surface modeling, based on automatically extracted stable points, to generate continuous distance correction fields.

Experimental results from a four-epoch TLS dataset collected by a permanent monitoring system in the Vals Valley (Austria) demonstrate that the proposed approach effectively mitigates inhomogeneous systematic errors that remain after registration. The M3C2-based analysis shows that the mean deviations in the upper region and the right side of the valley decrease by approximately 23–36%, while areas with small initial deviations remain nearly unchanged. Minor counter-effects observed in locally stable areas are below 0.5 mm and can be neglected.

Overall, the proposed method offers a straightforward and sensor-independent solution for compensating inhomogeneous systematic errors in TLS point clouds. It enhances the rigidity of point cloud data under complex atmospheric and topographic conditions without requiring auxiliary meteorological measurements, thereby improving the reliability of long-range TLS-based geodetic monitoring and the quality of subsequent deformation analysis.

Acknowledgements

This research was funded by the German Research Foundation (DFG) under the grant number 490989047, DFG FOR 5455 “TLS-Defo”.

References

Aichinger, J., Schwieger, V., 2022. Studies on deformation analysis of TLS point clouds using B-splines – A control point based approach (Part I). *Journal of Applied Geodesy*, 16(3), 279–298.

Anders, K., Winiwarter, L., Lindenbergh, R., Williams, J. G., Vos, S. E., Höfle, B., 2020. 4D objects-by-change: Spatiotemporal segmentation of geomorphic surface change from LiDAR time series. *ISPRS Journal of Photogrammetry and Remote Sensing*, 159, 352–363.

Bureick, J., Neuner, H., Harmening, C., Neumann, I., 2016. Curve and Surface Approximation of 3D Point Clouds. *Allgemeine Vermessungsnachrichten (AVN)*, 123, 315–327.

Czerwonka-Schröder, D., 2023. Konzeption einer qualitätsgesicherten Implementierung eines Echtzeitassistenzsystems basierend auf einem terrestrischen Long Range Laserscanner. PhD thesis, Technische Universität Bergakademie Freiberg, Germany.

Friedli, E., 2020. Point cloud registration and mitigation of refraction effects for geomonitoring using long-range terrestrial laser scanning. PhD thesis, ETH Zurich, Switzerland.

Friedli, E., Presl, R., Wieser, A., 2019. Influence of atmospheric refraction on terrestrial laser scanning at long range. *Proceedings of the 4th Joint International Symposium on Deformation Monitoring (JISDM)*, Athens, Greece, 15–17.

García-Asnejo, L., Lujan, R., Baselga, S., 2025. Mitigation of the refraction error in surveying techniques by using a network of meteorological sensors and a 3d refractivity model. *Proceedings of the 6th Joint International Symposium on Deformation Monitoring (JISDM)*, Karlsruhe, Germany.

Harmening, C., 2020. Spatio-temporal deformation analysis using enhanced B-spline models of laser scanning point clouds. Dissertation, TU Wien, Vienna, Austria.

Harmening, C., Butzer, R., 2024. Improving the approximation quality of tensor product B-spline surfaces by local parameterization. *Journal of Applied Geodesy*, 18(4), 575–596.

Harmening, C., Neuner, H., 2015. A constraint-based parameterization technique for B-spline surfaces. *Journal of Applied Geodesy*, 9(3), 143–161.

Harmening, C., Neuner, H., 2016. Choosing the Optimal Number of B-spline Control Points (Part 1: Methodology and Approximation of Curves). *Journal of Applied Geodesy*, 10(3), 139–157.

Harmening, C., Neuner, H., 2017. Choosing the optimal number of B-spline control points (Part 2: Approximation of surfaces and applications). *Journal of Applied Geodesy*, 11(1), 43–52.

Kermarrec, G., Kargoll, B., Alkhatib, H., 2020. Deformation Analysis Using B-Spline Surface with Correlated Terrestrial Laser Scanner Observations—A Bridge Under Load. *Remote Sensing*, 12(5), 829.

Kuschnerus, M., Lindenbergh, R., Vos, S., Hanssen, R., 2024. Statistically assessing vertical change on a sandy beach from permanent laser scanning time series. *ISPRS Open Journal of Photogrammetry and Remote Sensing*, 11, 100055.

Kuschnerus, M., Schröder, D., Lindenbergh, R., 2021. Environmental influences on the stability of a permanently installed laser scanner. *The International Archives of the Photogrammetry, Remote Sensing and Spatial Information Sciences*, 43, 745–752.

Lague, D., Brodu, N., Leroux, J., 2013. Accurate 3D comparison of complex topography with terrestrial laser scanner: Application to the Rangitikei canyon (NZ). *ISPRS Journal of Photogrammetry and Remote Sensing*, 82, 10–26.

Lindenbergh, R., Anders, K., Campos, M., Czerwonka-Schröder, D., Höfle, B., Kuschnerus, M., Puttonen, E., Prinz, R., Rutzinger, M., Voordendag, A. et al., 2025. Permanent terrestrial laser scanning for near-continuous environmental observations: Systems, methods, challenges and applications. *ISPRS Open Journal of Photogrammetry and Remote Sensing*, 100094.

Luján, R., García-Asenjo, L., Baselga, S., 2025. Three-dimensional refractivity model for atmospheric mitigation in distance and vertical angle measurements. *Sensors*, 25(7), 1981.

Ötsch, E., Harmening, C., Neuner, H., 2023. Investigation of space-continuous deformation from point clouds of structured surfaces. *Journal of Applied Geodesy*, 17(2), 151–160.

Piegl, L., Tiller, W., 1995. *The NURBS Book*. Monographs in Visual Communications, Springer Berlin Heidelberg, Berlin, Heidelberg.

Schröder, D., Anders, K., Winiwarter, L., Wujanz, D., 2022. Permanent terrestrial lidar monitoring in mining, natural hazard prevention and infrastructure protection–chances, risks, and challenges: A case study of a rockfall in tyrol, austria. *Proceedings of the 5th Joint International Symposium on Deformation Monitoring (JISDM)*, Editorial Universitat Politècnica de València, Valencia, Spain.

Soudarissanane, S., Lindenbergh, R., Menenti, M., Teunissen, P., 2011. Scanning geometry: Influencing factor on the quality of terrestrial laser scanning points. *ISPRS Journal of Photogrammetry and Remote Sensing*, 66(4), 389–399.

Voordendag, A., Goger, B., Klug, C., Prinz, R., Rutzinger, M., Sauter, T., Kaser, G., 2023. Uncertainty assessment of a permanent long-range terrestrial laser scanning system for the quantification of snow dynamics on Hintereisferner (Austria). *Frontiers in Earth Science*, 11, 1085416.

Yang, Y., 2023. Towards improved targetless registration and deformation analysis of TLS point clouds using patch-based segmentation. PhD thesis, Universität Stuttgart, Stuttgart, Germany.

Yang, Y., Czerwonka-Schröder, D., Seufert, P., Holst, C., 2025. Using point cloud registration to mitigate systematic errors in permanent laser scanning-based landslide monitoring. *Proceedings of the 6th Joint International Symposium on Deformation Monitoring (JISDM)*, Karlsruhe, Germany.

Yang, Y., Holst, C., 2025a. How to Find Geometric Changes in Laser Scanning Point Clouds? A Perspective on Correspondence Definitions. *ISPRS Annals of the Photogrammetry, Remote Sensing and Spatial Information Sciences*, 1003–1010.

Yang, Y., Holst, C., 2025b. Piecewise-ICP: Efficient and robust registration for 4D point clouds in permanent laser scanning. *ISPRS Journal of Photogrammetry and Remote Sensing*, 227, 481–500.